Clin Transl Imaging (2014) 2:427–437
DOI 10.1007/s40336-014-0078-7

REVIEW ARTICLE

Opportunities for nanotheranosis in lung cancer and pulmonary metastasis

J. Key · Y.-S. Kim · F. Tatulli · A. L. Palange · B. O'Neill · S. Aryal · M. Ramirez · X. Liu · M. Ferrari · R. Munden · P. Decuzzi

Received: 14 July 2014 / Accepted: 16 August 2014 / Published online: 27 August 2014

Abstract Malignancies of the lungs, both primary and metastatic, are the leading cause of death worldwide. Over 1.5 million new cases of primary lung cancer are diagnosed annually worldwide with a dismal 5-year survival rate of approximately 15 %, which remains unchanged despite major efforts and medical advances. As expected, survival for patients with lung metastases is even worse at about 5 %. Early detection and staging are fundamental in improving survival rates and selecting the most effective treatment strategies. Recently, nanoparticles have been developed for imaging and treating various cancers, including pulmonary malignancies. In this work, three different examples of nanoparticle configurations for cancer theranosis are presented, namely conventional spherical polymeric nanoparticles with a diameter of ~150 nm; and discoidal mesoporous silicon nanoconstructs and discoidal polymeric nanoconstructs with a diameter of ~1,000 nm and a height of 400 and 500 nm, respectively. The spherical nanoparticles accumulate in tumors by means of the well-known enhanced permeation and retention effect, whereas sub-micrometer discoidal nanoconstructs are rationally designed to adhere firmly to the tortuous tumor vasculature. All three nanoparticles are characterized for their in vivo performance in terms of magnetic resonance, positron-emission tomography (PET), and optical imaging. Preliminary data on the in vivo and ex vivo PET/CT imaging of breast cancer metastasis in the lungs using discoidal nanoconstructs is presented. In conclusion, opportunities for nanoparticle-based theranosis in primary lung cancer and pulmonary metastasis are presented and discussed.

Keywords Nanoparticles · Multi-modal imaging · Nanomedicine

Color figures online at http://link.springer.com/article/10.1007/s40336-014-0078-7

J. Key · Y.-S. Kim · A. L. Palange · B. O'Neill · S. Aryal · M. Ramirez · P. Decuzzi (✉)
Department of Translational Imaging, Houston Methodist Research Institute, Houston, TX 77030, USA
e-mail: pdecuzzi@houstonmethodist.org; paolo.decuzzi@iit.it

F. Tatulli
PET Center, Houston Methodist Research Institute, Houston, TX 77030, USA

X. Liu · M. Ferrari
Department of Nanomedicine, Houston Methodist Research Institute, Houston, TX 77030, USA

R. Munden
Department of Radiology, Houston Methodist Hospital, Houston, TX 77030, USA

P. Decuzzi
Department of Drug Discovery and Development, Fondazione Istituto Italiano di Tecnologia, 16163 Genoa, Italy

Introduction

Primary and secondary malignancies developing in the lungs are among the world's leading cancer killers. Primary lung cancer annually accounts for 7.6 million deaths worldwide and, in 2014, about 160,000 Americans are expected to die from this disease, corresponding to approximately 27 % of all cancer deaths [1, 2]. The 5-year survival rate for lung cancer is only 15 %, which is much lower than for many other malignancies. For lung cancers detected at an early stage, survival dramatically improves with stage I survival as high as 77 % [3]. However, only 15 % of lung cancers are diagnosed at an early stage. The picture is far more complex as regards secondary tumors developing in the lungs, which show a 5-year survival rate of only 4 %. Contrary to other

malignancies, the number of deaths due to primary and secondary lung cancers has steadily increased over the last 10 years [4]. Because of their fine microvascular network, the lungs are among the most frequent sites of metastases from extra-thoracic malignancies. Therefore, if primary lung cancer is mostly considered a disease of older heavy smokers [5], pulmonary metastasis affects all age groups. Pulmonary metastatic disease, originating from primary tumors at other sites, is seen in 20–50 % of extra-thoracic malignancy cases [6]. Pulmonary metastasis originates from practically any primary tumor, most commonly from lung, skin (melanoma), bone (osteosarcoma), bladder, prostate, breast, colon, and kidney cancers, among others.

Given the relatively high survival rates for early-detected cases, accurate staging of tumors developing in the lungs is important for selecting the most effective treatment plan and improving outcomes. Relatively small tumors are generally resectable unless they are located in critical areas, whereas large tumors and pulmonary metastasis are treated with metastectomy, radiation therapy, chemotherapy, or combination therapy [7]. Clinically relevant imaging modalities for staging lung cancers and identifying pulmonary metastasis are chest radiographs (CXR), computed tomography (CT), and fused positron-emission tomography CT (PET/CT). Chest radiography (CXR) is the most commonly used imaging modality and often the first modality used in assessing the lungs for pulmonary metastasis from many non-thoracic primary malignancies. However, chest radiographs have low sensitivity, especially for primary lung cancer. Low-dose CT is now the recommended modality for early detection of primary lung cancer [8]; diagnostic CT is the primary method used for staging many non-thoracic malignancies. However, long-term use of CT for surveillance of metastatic lung disease is not common because of the expense and potential radiation dose exposure [9]. Also, CT guidance is often required for radiation therapy and histological sampling. Whole-body PET using ^{18}F-deoxyglucose (FDG) has also become a very useful tool in staging primary lung cancer as well as many non-thoracic malignancies; and fused PET/CT imaging is now the standard FDG modality because of its improved performance over PET alone and over conventional staging methods [10–12].

In cancer imaging and therapy, nanoparticles (NPs) have been proposed as agents for disease detection, treatment and follow-up of therapy. NPs are man-made objects small enough to be injected intravascularly and navigate safely within the circulatory system, and they are designed to perform several, useful functions [13, 14]. They can efficiently carry multiple, and different, imaging and therapeutic molecules from the site of injection to the biological target (malignant tissue), where they provide contrast enhancement and exert a curative action. A large variety of NPs having different sizes, shapes, surface properties, and compositions have been developed for diverse oncological applications. It is important to recall that colloidal formulations of different materials are already approved and routinely used in the clinic for cancer imaging and therapy. For instance, the intravenous administration of technetium ^{99m}Tc–sulfur colloids is employed in delineating the lymphatic drainage from primary tumors and in localizing sentinel nodes in breast cancer and melanoma. Tiny glass beads, filled with the radioisotope yttrium-90, are used for the radioembolization of malignancies growing in the liver. However, aspects of the in vivo performance of the most recently developed NPs, such as their circulation half-life and organ biodistribution, can be finely tuned by precisely controlling, during synthesis, their geometrical and physico-chemical properties.

Here, after introducing the notion of NPs and their applications in the field of cancer imaging and therapy (theranosis), this work presents three different examples of NPs developed by the authors and discusses recent preliminary data on the multi-modal imaging of pulmonary breast cancer metastasis.

Nanoparticles for cancer theranosis

In cancer imaging and therapy, the advantage of using NPs over freely administered molecules can be summarized in the following two points: (1) the size, shape, surface properties and composition of NPs can be finely tuned, during synthesis, to enhance their accumulation at the diseased site while limiting off-site targeting (engineerability of nanoparticles); (2) multiple and different therapeutic and imaging molecules can be simultaneously loaded within the same NP, without interfering with the original organ-specific biodistribution (multi-functionality of nanoparticles).

The main paradigm in the design of NPs for oncological applications is based on the observation that the tumor vasculature is discontinuous and presents openings (fenestrations) measuring several hundreds of nanometers. NPs, typically being smaller than 200 nm, progressively accumulate within the tumor tissue by crossing these endothelial fenestrations (Fig. 1) [15]. This phenomenon, first documented by Maeda in 1989 [16], is generally known as the enhanced permeation and retention (EPR) effect. The majority of NPs described in the literature over the last 20 years are designed according to this paradigm. Unfortunately, however, organs of the reticulo-endothelial system, such as the liver, spleen, and bone marrow, are also characterized by a discontinuous endothelium and tend to avidly sequester foreign circulating objects, including NPs. Consequently, only a small fraction of injected NPs ultimately accumulates at the diseased site. Generally this is in the order of 1 % of the injected dose per gram tumor

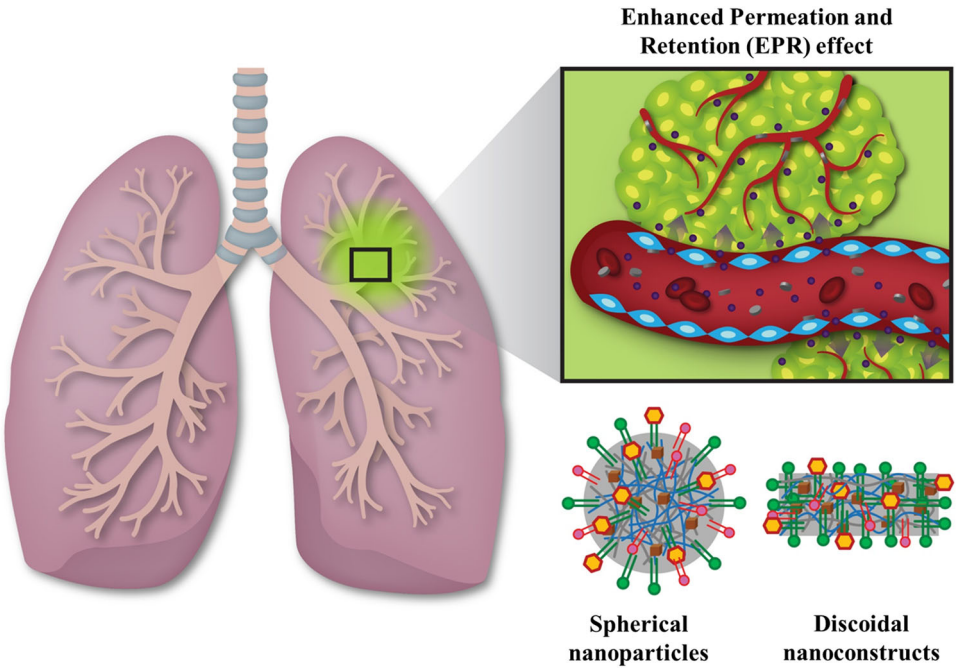

Fig. 1 Delivery of nanoparticles to cancers developing in the lungs. Spherical nanoparticles, typically smaller than 200 nm in size, accumulate within tumor tissue by crossing endothelial fenestrations, whereas sub-micron discoidal nanoconstructs are designed to lodge within the tortuous tumor vasculature without relying on the enhanced permeation and retention (EPR) effect. *Spherical nanoparticles* and *discoidal nanoconstructs* can be loaded with a variety of chemotherapeutic molecules (such as doxorubicin, docetaxel, paclitaxel), and with multiple imaging agents, including infra-red and near infra-red dyes (for optical imaging), Gd^{3+}-ions and iron oxide nanocrystals (for magnetic resonance imaging), radioisotopes (for nuclear imaging), and iodine molecules and gold nanoparticles (for CT imaging) (color figure online)

(% ID/g). Nonetheless, this is a much larger proportion than the typical accumulation dose of freely injected molecules, and it has been demonstrated to be sufficient for successfully treating cancer in several animal models and, in a few cases, also in humans [14].

Besides fenestrations, tumor masses are also characterized by a tortuous vascular network, low mean blood velocity, impaired lymphatic system, and high interstitial fluid pressure [15]. In particular, the mean blood velocity in most tumors is 1–10 μm/s, which is about ten times lower than that recorded in healthy vessels [15]. Taking advantage of this, our group has proposed sub-micron, discoidal nanoconstructs as vehicles for preferentially targeting the malignant vasculature, without relying on the EPR effect (Fig. 1) [17]. Unlike small NPs, these discoidal nanoconstructs are designed to recognize the altered tumor vasculature and to adhere firmly to the endothelial walls, without crossing the fenestrations [18, 19]. They are sub-micron in size and tend to be pushed laterally in the so-called cell-free layer by the fast moving red blood cells. Therefore, by design, these nanoconstructs tend to move in close proximity to the vessel walls, continuously sensing for local vascular abnormalities [20]. Also, the discoidal shape of these nanoconstructs favors firm, stable adhesion to the vessel walls in regions of lower blood velocity [18, 19].

Both conventional spherical NPs and discoidal nanoconstructs can be loaded with a variety of drug molecules, including potent chemotherapeutic molecules, such as doxorubicin, docetaxel, paclitaxel [21–23], and labeled with multiple contrast agents, including infra-red and near infra-red dyes (for optical imaging) [22]; Gd^{3+}-ions and iron oxide nanocrystals (for magnetic resonance imaging: MRI) [23–27]; radioisotopes (for nuclear imaging) [28]; and iodine molecules and gold nanoparticles (for CT imaging).

Spherical polymeric nanoparticles

Nanoparticles for oncological applications are generally spherical in shape and exhibit a diameter of up to about 200 nm. These NPs are synthesized via a bottom-up approach where the different constituents (i.e., lipid and polymer chains) spontaneously assemble via inter-molecular interactions to form larger constructs. Therapeutic molecules are generally dispersed within the NP core during the synthesis process, whereas imaging molecules are attached to the NP surface at the end of the process.

Our group has been synthesizing spherical, polymeric-phospholipid NPs by means of a nano-precipitation method [28]. These NPs present a hydrodynamic diameter of about

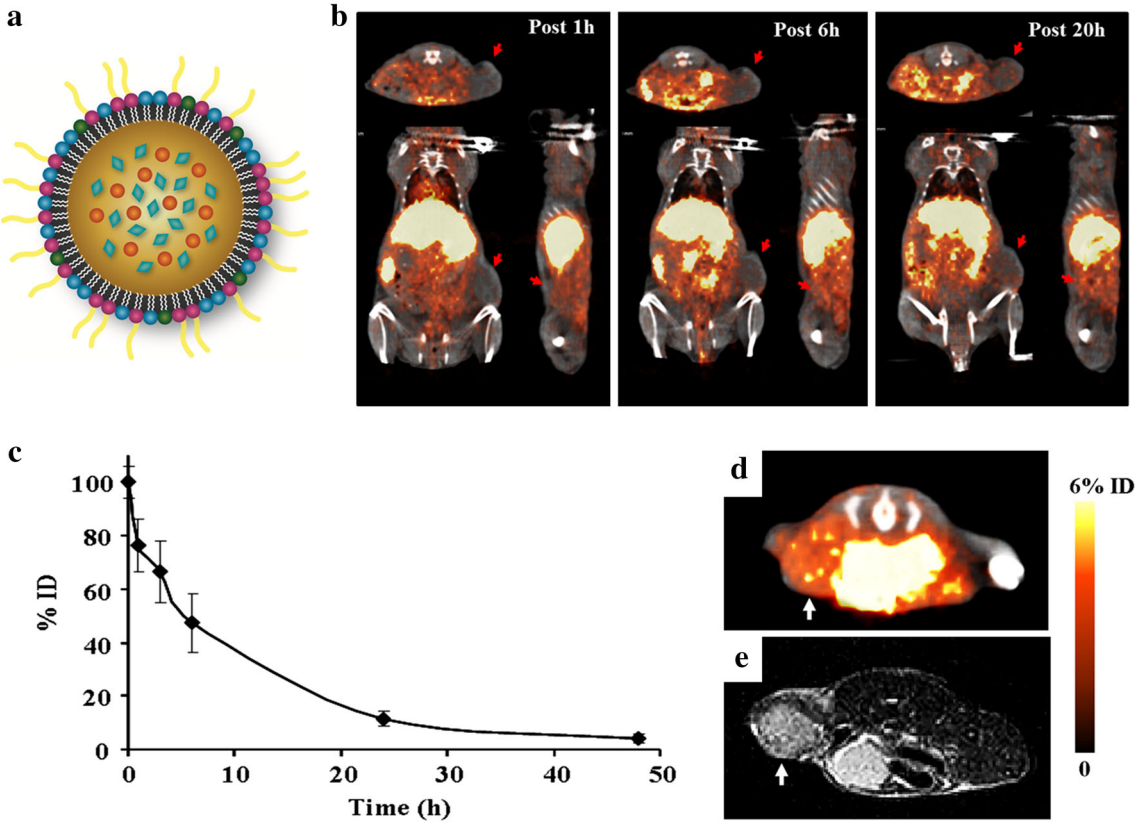

Fig. 2 Cancer imaging with spherical polymeric nanoparticles. **a** Schematic representation of polymeric-phospholipid nanoparticles, exhibiting a hydrodynamic diameter of ~150 nm. The polymeric core is stabilized by a monolayer of lipids and PEG chains, visible in the diagram. **b** PET/CT imaging of breast tumor-bearing mice following systemic injection of 100 μCi of spherical nanoparticles labeled with ^{64}Cu(DOTA). **c** Percentage of the injected dose of spherical nanoparticles in the blood pool as a function of time, determined via scintillation counting. **d**, **e** PET imaging and MRI of spherical nanoparticles accumulating within the breast tumor tissue at ~20 h p.i. Nanoparticles mostly accumulate at the periphery of the malignant mass, as dictated by the EPR effect. Rearranged from Aryal et al. [28] (color figure online)

150 nm, a ξ-potential of −35.0 mV, and are sufficiently small to rely on the EPR effect for tumor accumulation [29–31]. A schematic representation of this type of NP is presented in Fig. 2a. In this configuration, NPs comprise three different compartments: a poly(lactic-*co*-glycolic acid) (PLGA) core, encapsulating 5 nm ultra-small superparamagnetic iron oxide nanocrystals (USPIOs); a middle compartment, composed of a single phospholipid layer which can be labeled with radionuclides (^{64}Cu) and optical probes; and an outer compartment, composed of poly(ethylene glycol) (PEG) chains, conferring long residence times in blood. The phospholipid monolayer and the PEG chains also serve to stabilize the PLGA core. In the present configuration, Cu^{2+}-ions are stably chelated to the lipid monolayer via a DOTA cage, so that the resulting NPs can carry, simultaneously, USPIOs for MRI and ^{64}Cu(DOTA) for PET imaging. For this reason, the resulting NPs are named positron-emitting magnetic nanoconstructs (PEMs). In addition to being used as contrast agents, PEMs have also been loaded with drug molecules, such as docetaxel and rosiglitazone for the treatment of tumors and atherosclerosis, respectively [29].

Following their injection into mice bearing breast tumors (MDA-MB-231), the distribution of PEMs in various organs is monitored over time using a micro-PET/CT scanner (Siemens Inveon) (Fig. 2b). Actually, the same analysis can also be performed in other tumors, including primary and secondary malignancies developing in the lungs, as shown later. Images were taken at 1, 6, and 20 h post-injection (p.i.). Within 1 h p.i., high activity is detected in the lungs, heart and organs of the abdominal cavity, particularly the liver and spleen. However, over time, this signal reduces while the activity in the malignant mass steadily grows. This behavior has to be ascribed to the long circulation properties of PEMs that reside in the blood pool for several hours p.i. and progressively accumulate within the malignant mass via the EPR effect. Interestingly, the activity in the digestive system also increases over time suggesting that PEMs are metabolized in the liver and follow the biliary excretion route. Because of the surface

PEG shielding, PEMs tend to reside in the blood pool for several hours, presenting a circulation half-life of about 6 h as determined via scintillation counting (Fig. 2c). This is certainly longer than the average residence time of ^{64}Cu(DOTA) in blood which amounts to only a few minutes [30].

After completing PET scanning, at 20 h p.i. mice underwent MRI in a clinical 3T scanner (Philips Ingenia®). Figure 2d presents PET/CT and MR images of the sole tumor at 20 h p.i. The images show focal areas of ^{64}Cu activity corresponding to focal areas of reduced T_2* signal on MR images, confirming that the nanoparticles are still intact within the tumor mass. Also, the highest PEM concentrations are reached at the periphery of the tumor mass, confirming that the accumulation of PEMs is mostly associated with the EPR effect. After animal sacrifice, a biodistribution study was conducted by harvesting the major organs (liver, spleen, kidneys, lungs, heart, brain, and the tumor) and quantifying residual radioactivity using a gamma counter (PerkinElmer®). The PEM accumulation in the tumor was in the order of 4 % ID/g, which is consistent with the literature data for most NPs. Also, as expected, the highest tissue accumulations were observed in the liver and spleen, corresponding to about 20 and 5 % ID/g, respectively.

Discoidal mesoporous silicon nanoconstructs

These nanoconstructs, schematically represented in Fig. 3a, are discoidal in shape and have a diameter of 1,000 nm and a height of 400 nm. Unlike conventional spherical NPs, these discoidal nanoconstructs are fabricated using a top-down approach, as detailed by the authors in a previous work [24, 31]. Briefly, the geometry (size and shape) of the nanoconstructs is defined by photolithography, whereas the mesoporous structure is obtained via electrochemical etching. Nanoconstructs with various geometries can be fabricated by changing the photolithographic parameters, while the pore size can be finely adjusted to range from $\sim$10 nm (small pore) to $\sim$60 nm (huge pore). The mesoporous structure of these nanoconstructs has been efficiently loaded with several agents for cancer treatment and imaging. For instance, paclitaxel-containing polymer micelles and nanoliposomes carrying siRNAs have been successfully encapsulated into silicon pores and used for the treatment of breast cancer [32–34]. Also, the authors have loaded gadolinium-(diethylene triamine pentaacetic acid) Gd(DTPA) molecules into the silicon mesoporous structure for MRI [24, 25]. In this case, it has been shown that the geometrical confinement of Gd(DTPA) within the mesopores is responsible for enhancing the longitudinal relaxivity r_1 of the Gd^{3+}-ions leading to an approximately fourfold increase, as compared to the same free molecules in a bulk solution. More recently, the authors have also conjugated Gd(DOTA) molecules directly to the silicon surface demonstrating longitudinal relaxivities of up to 20 $(mM\ s)^{-1}$, at 1.41 T [35]. This enhancement in relaxivity for Gd(DTPA) and Gd(DOTA) has to be ascribed to the increase in both rotational correlation time (τ_R) (inner-sphere effect) for the Gd^{3+}-ions and diffusion correlation time (τ_D) for the water molecules (outer-sphere effect within the silicon mesopores) [24].

Following the results obtained with Gd-based macro molecules, the authors also studied the confinement of USPIOs within porous matrices. Following the loading of 5 nm USPIOs within the mesoporous matrix of the discoidal silicon nanoconstructs (Fig. 3a, b), the transverse relaxivity (r_2) was characterized using a bench-top relaxometer (1.41 T). In this case, too, a considerable (almost threefold) enhancement in relaxivity was observed, returning discoidal silicon nanoconstructs with an r_2 of up to 350 $(mM\ s)^{-1}$ [27]. In this case, the observed enhancement in transverse relaxivity has to be ascribed to the different hydration conditions of the USPIOs within the mesopores of the silicon nanoconstructs (see TEM and EDX analysis in Fig. 3b). Phantom images of the USPIO-loaded discoidal nanoconstructs with different iron contents are presented in Fig. 3c, as obtained using a clinical 3T MRI scanner (Philips Ingenia®).

Importantly, given the sub-micrometer size of the discoidal nanoconstructs, over 4.0×10^4 USPIOs of 5 nm size can be loaded into a single nanoconstruct thus providing a huge, localized concentration of Fe. This can be efficiently used to guide, in vivo, the magnetic nanoconstructs and maximize their accumulation at the tumor site. This is demonstrated in the MR images shown in Fig. 3d obtained in three different experimental groups of animals bearing a melanoma tumor (B16–F10). Specifically, the top row relates to the systemic injection of free 5 nm USPIOs, in the presence of an external magnet; the middle row to discoidal silicon nanoconstructs loaded with USPIOs, in the absence of an external magnet; and the bottom row to discoidal silicon nanoconstructs loaded with USPIOs, in the presence of an external magnet. In all cases, the magnet was placed on the tumor side for 4 h p.i. The same amount of iron was injected for all three groups, corresponding to $\sim$0.5 mg of Fe/kg (8 μg of USPIOs per mouse), which is one order of magnitude lower than the amounts generally injected for MRI. The mice were imaged pre-injection, after removal of the magnet at 4 h p.i., and just before killing at 24 h p.i, using a clinical 3T MRI scanner. For the free USPIOs, no statistically significant difference in intensity ratio was observed over time, most likely due to the low injected dose. On the other hand, for the discoidal nanoconstructs, dragged by a magnet, a significant drop in

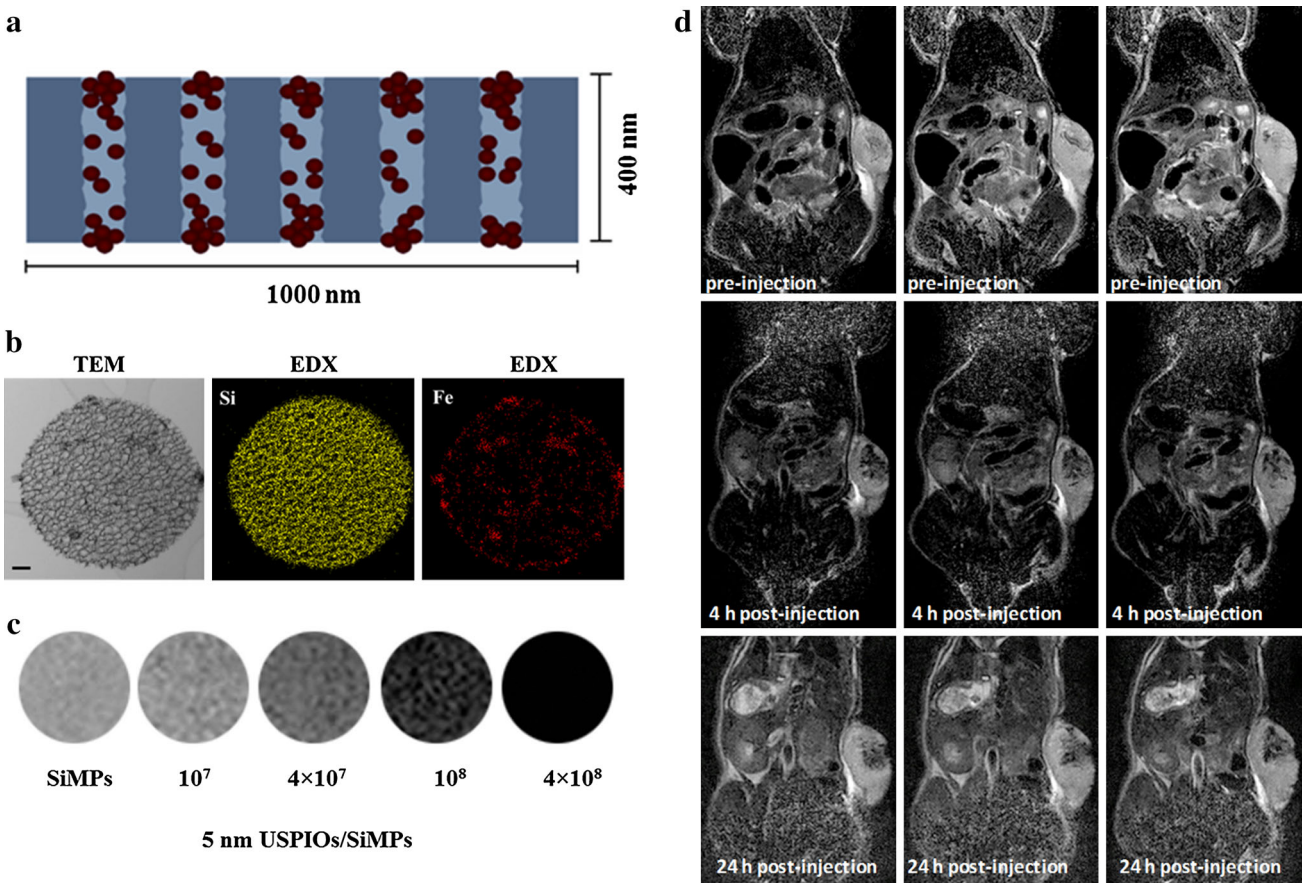

Fig. 3 Cancer imaging with discoidal mesoporous silicon nanoconstructs. **a** Schematic representation of discoidal mesoporous silicon nanoconstructs, loaded with iron oxide nanocrystals (USPIOs: *red beads*). In this configuration, the average pore size of the silicon matrix is 40 nm. **b** Transmission electron micrographs and energy-dispersive X-ray spectroscopy imaging of the discoidal nanoconstructs for silicon (Si) and iron (Fe). **c** MRI phantom images of the discoidal nanoconstructs, showing different iron concentrations (at 3T). **d** MR imaging of melanoma tumor-bearing mice following systemic injection of free 5 nm UPIOs, in the presence of a magnet (*top*); discoidal nanoconstructs loaded with USPIOs, in the absence of a magnet (*middle*); discoidal nanoconstructs loaded with USPIOs, in the presence of a magnet (*bottom*) (injected dose: ~0.5 mg of Fe/kg animal). Rearranged from Gizzatov et al. [27] (color figure online)

intensity ratio, up to 60 %, was observed within the first 4 h. This finding demonstrates that magnetic dragging with such sub-micrometer nanoconstructs can be efficiently used to enhance tumor accumulation and thus increase delivery doses.

Discoidal polymeric nanoconstructs

Discoidal polymeric nanoconstructs (DPNs) are our third example of NPs for cancer theranosis. DPNs are synthesized using a top-down approach combining electron beam lithography and polymer chemistry, as described by the authors in a previous work [22]. The fabrication process starts with the definition of a geometrical pattern of wells in a master silicon template, using lithographic techniques. The well represents the final geometry of the nanoconstruct. From the silicon template, sacrificial templates are originated for the actual DPN synthesis. Figures 4a, b present scanning electron micrographic (SEM) and optical fluorescence images of DPNs still adhering to a sacrificial template. DPNs are seen to be arranged in an orderly fashion in rows and columns, which are about 3,000 nm apart, and they present a diameter of ~1,000 nm. The upper-right insets in both images present details of the DPN geometry. A transmission electron micrograph of DPNs demonstrates the presence of 5 nm USPIOs (black spots) within the polymeric matrix (Fig. 4c). In this specific configuration, DPNs are obtained by photo-polymerizing a polymeric paste comprising PLGA chains, multi-arm PEG acrylate chains, lipid-DOTA chains, lipid-Rhodamine B dye (RhB), and USPIOs. While RhB and USPIOs are used for providing the optical and MRI capabilities, the lipid-DOTA chains, uniformly distributed within the polymer matrix, are reacted with copper chloride salts after DPN formation to generate Cu^{64}-DPNs for PET imaging.

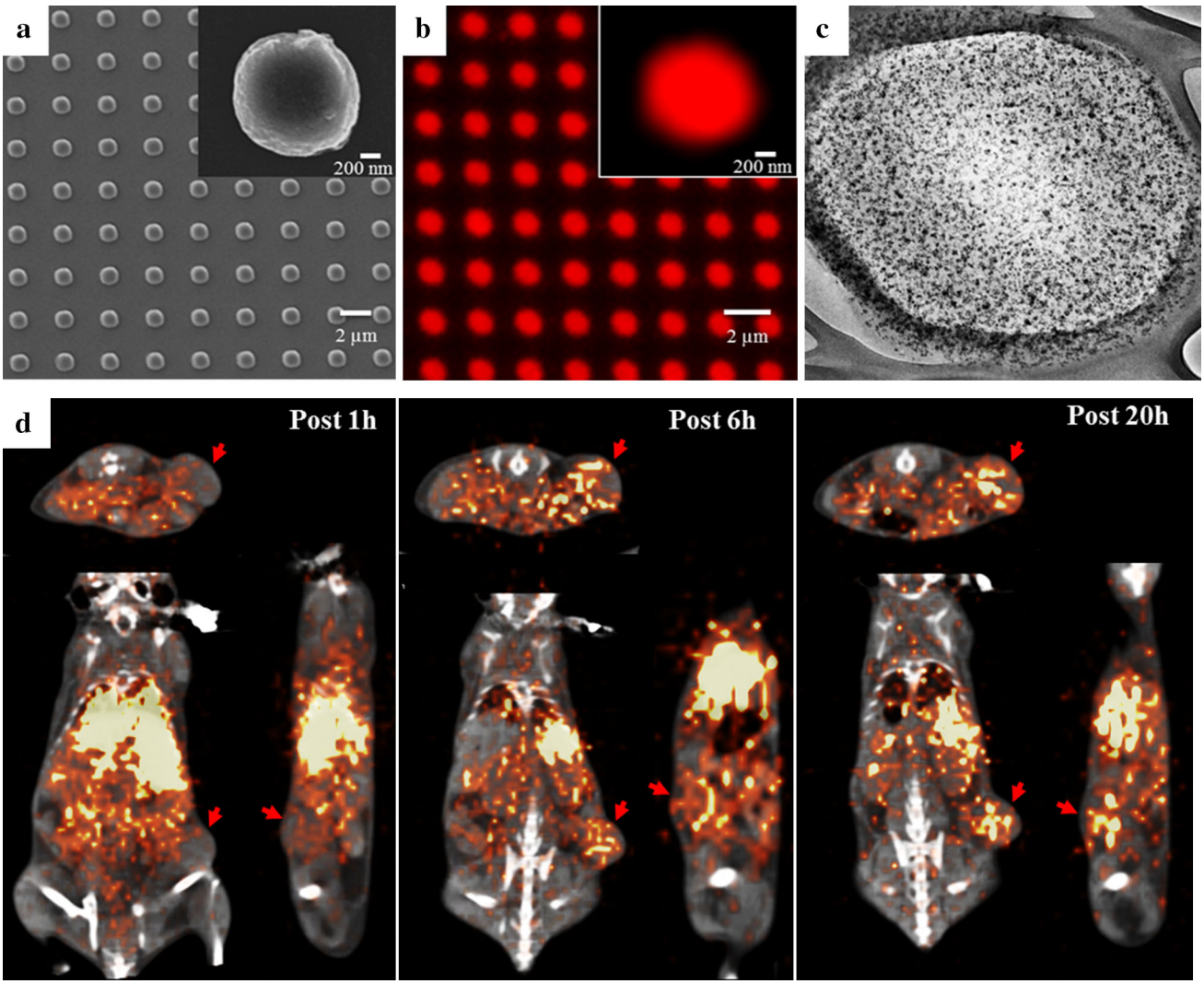

Fig. 4 Cancer imaging with discoidal polymeric nanoconstructs. **a**, **b** Scanning electron micrographic (SEM) and optical fluorescence images of discoidal polymeric nanoconstructs, lying in an orderly fashion over a polymeric sacrificial template. **c** Transmission electron micrograph of discoidal polymeric nanoconstructs loaded with 5 nm iron oxide nanocrystals (*black dots*). **d** PET/CT imaging of breast tumor-bearing mice following systemic injection of 50 μCi of discoidal polymeric nanoconstructs labeled with ^{64}Cu(DOTA) (color figure online)

These polymeric nanoconstructs have been used to image breast (MDA-MB-231), brain (U87-MG), and melanoma (B16-F10) tumors. In the case of breast cancer (Fig. 4d), PET/CT imaging was performed at different time points, namely 1, 6, 20 h p.i., in order to follow longitudinally the in vivo behavior of DPNs. Images are normalized by the injected dose and corrected for the decay time of the radioisotope so that they can be directly compared. As expected for any nanoparticle, within the first hour p.i., a significant activity is detected in the lungs. This reduces over time as the DPNs are washed away from the pulmonary microvasculature. A significant activity is also observed in the abdominal cavity, and it is again associated mostly with the long residence time of DPNs in the circulation. More importantly, as time progresses, the activity in the malignant mass (right flank) grows consistently. As DPNs escape the lung microvasculature and pass through the highly perfused liver and abdominal organs, they progressively lodge within the tumor vasculature reaching unprecedented accumulation doses at 48 h p.i. DPNs exhibit a circulation half-life of almost 24 h (data not shown).

Given the initial, transient accumulation of DPNs in the lungs, these same nanoconstructs have been considered for preliminary imaging studies of pulmonary tumors. The hypothesis is that DPNs would permanently deposit in the tortuous vasculature of pulmonary tumors. In order to verify this hypothesis, pulmonary metastasis of breast cancer has been originated by injecting MDA-MB-231/Luc cells (1×10^5 cells) into mice, via the tail vein. The cancer

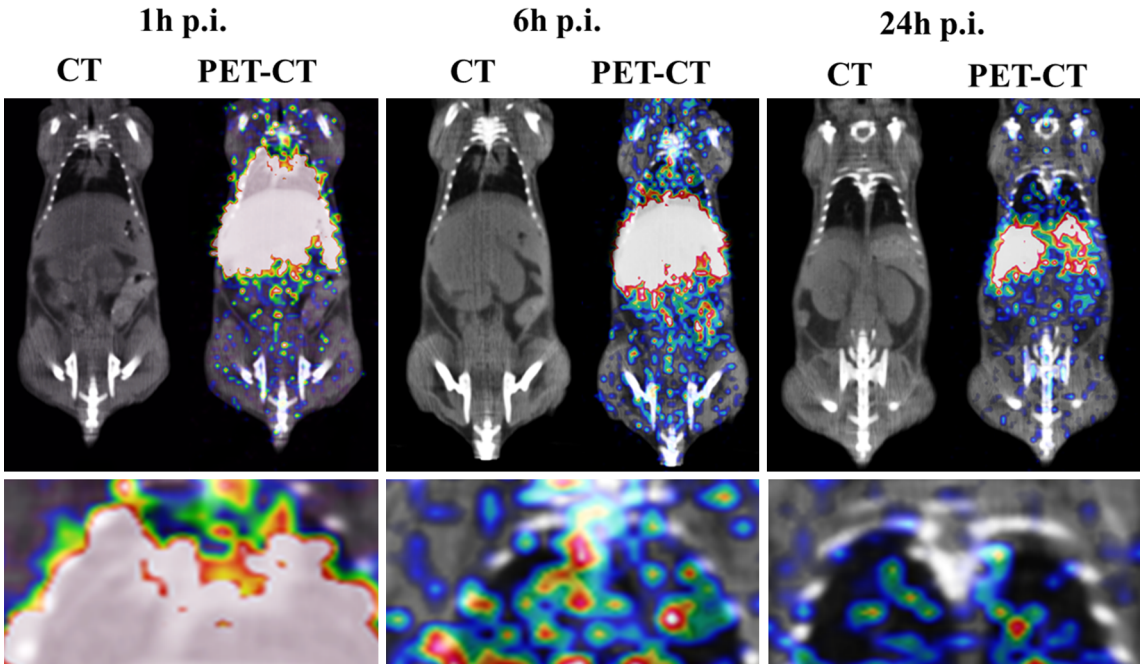

Fig. 5 PET/CT imaging of pulmonary metastasis with discoidal nanoconstructs. PET/CT imaging of mice, bearing breast cancer metastasis in the lungs, following systemic injection of 50 μCi of discoidal polymeric nanoconstructs labeled with ^{64}Cu(DOTA). Images are taken at 1, 6 and 24 h post-injection and show the presence of hot spots in the lungs at the later time point (24 h), possibly associated with metastasis. The liver activity reduces progressively over time. Note that PET images are corrected for the decay time of the radioisotope so that they can be directly compared (color figure online)

cells express luciferase and can therefore be conveniently imaged to monitor tumor development within the lungs. Figure 5 shows PET/CT images of murine lungs taken at 1, 6 and 24 h p.i. Within the first 1 h p.i., the signal in the lungs is saturated and progressively reduces over time leaving a few host spots at 24 h p.i. Figure 6a shows the accumulation of MDA-MB-231/Luc cells within the lungs of a living mouse. These cells require 3–5 weeks to develop into pulmonary nodules. Figure 6b–d shows ex vivo images of harvested lungs acquired via bioluminescence (BL) (Fig. 6b), which identifies the location of the metastasis; PET/CT (Fig. 6c), which serves to localize DPNs and quantify their accumulation in the microvasculature; and optical imaging, which helps in delineating regions with multiple tumor nodules (yellow arrows in Fig. 6d). The spatial distribution of the hot spots observed via BL, PET/CT, and the surface nodules correlates well. In particular, a large metastatic site is identified in the upper portion of the right lung, as confirmed by the pictures in Fig. 6b–d, and seems to correlate with the PET hot spot detected in the live animal at 24 h (Fig. 5). Although still preliminary, these data demonstrate the potential of DPNs for detecting lung malignancies simply by exploiting the altered vascular structure and blood perfusion within the pulmonary cancer nodules.

Future directions and opportunities

Nanoconstructs can improve the bioavailability and biodistribution of systemically injected agents by exploiting the altered architecture and biology of the tumor vasculature. The size, shape, surface properties, and composition of nanoconstructs can be tailored during the fabrication process to support their preferential deposition within the tumor vasculature or passive permeation through tumor fenestrations (engineerability). Also, nanoconstructs can encapsulate large amounts of different therapeutic and imaging agents (multi-functionality).

For tumor imaging, nanoconstructs can be loaded with USPIOs and tagged with Gd-based macromolecules [Gd(DOTA), Gd(DTPA)] for MRI; labeled with different types of radionuclides (^{18}F, ^{64}Cu) for PET and (^{99}Tc, ^{111}In) SPECT imaging; decorated with a variety of dyes (RhB, Cy5.5) for optical imaging; and loaded with iodine molecules and gold nanoparticles for CT imaging. All these modalities (MRI, PET, SPECT, optical, CT) can coexist within the same nanoconstructs, without interfering with any moieties for molecular targeting, thus nanoconstructs enable both multi-modal and molecular imaging. For cancer therapy, NPs can deliver multiple agents providing different curative approaches. Potent chemotherapeutic

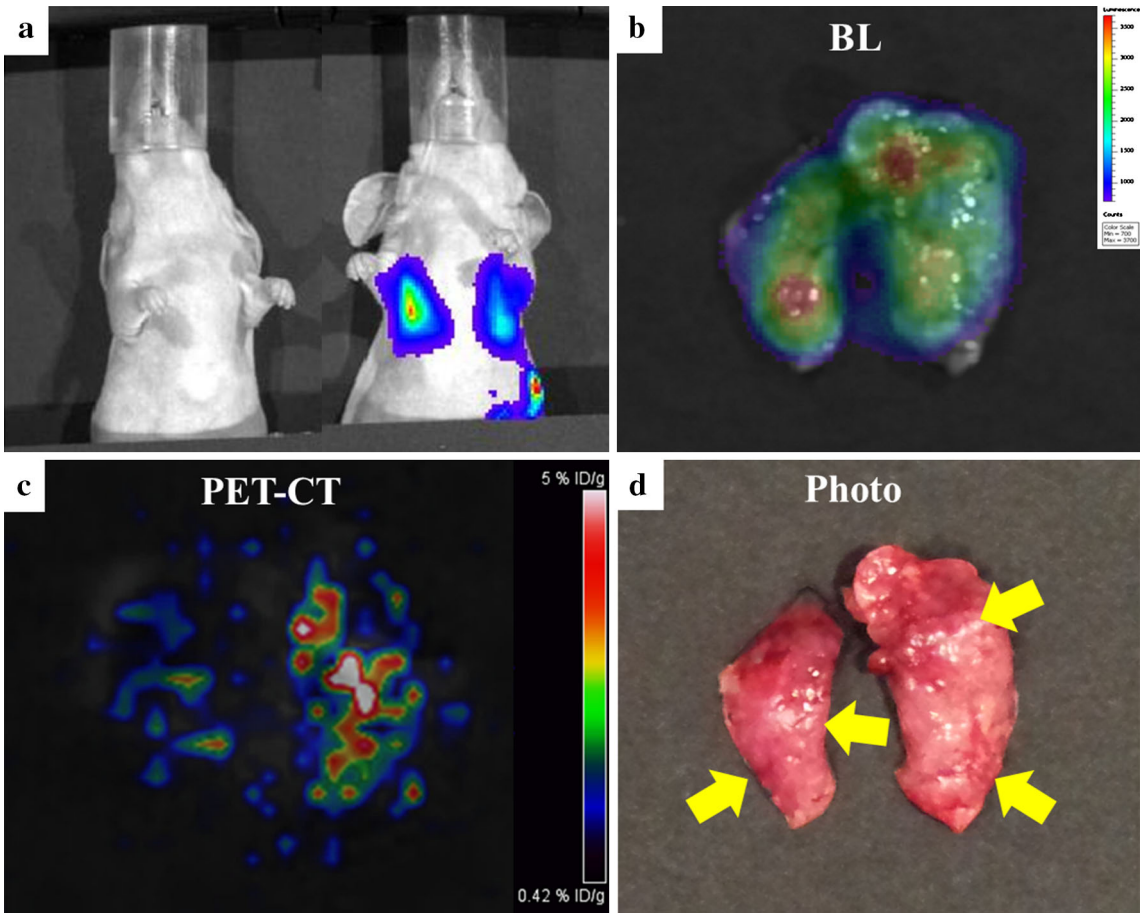

Fig. 6 Ex vivo imaging of pulmonary metastasis with discoidal nanoconstructs. **a** Bioluminescence imaging of MDA-MB-231/Luc cells forming pulmonary metastasis in the right and left lungs of a mouse (*right*). The control mouse (*left*), which was not injected with tumor cells, shows no bioluminescence signal. The MDA-MB-231/Luc cells are injected via the tail vein ($\sim 10^6$ cells) and require 3–5 weeks to develop stably growing pulmonary metastasis. **b** Bioluminescence imaging of the harvested lungs showing clusters of tumor cells in the *upper portion* of the right lung and *lower portion* of the left lung. **c** PET/CT imaging of the harvested lungs showing *hot spots* in the *upper* and *central* portions of the right lung and *central* and *lower* portions of the left lung. **d** Photograph of the harvested lungs showing regions (*yellow arrows*) with multiple nodules on the right and left lungs (color figure online)

molecules, such as doxorubicin, docetaxel, paclitaxel, and so on, can be encapsulated within the same nanoconstructs and released, at the diseased site, following precise schedules. In addition, metal nanoparticles, such iron oxide and gold nanoparticles, loaded into the nanoconstructs can deploy, upon external excitation, significant doses of thermal energy to induce localized hyperthermia and tissue ablation. Indeed, truly combinatorial drug delivery and synergistic therapies can be achieved only by using nanoconstructs.

Specifically, for the imaging and treatment of lung tumors and pulmonary metastasis, different nanoconstruct configurations can be envisioned which could improve on the current clinically available intervention protocols. For instance, sub-micrometer discoidal nanoconstructs can be tagged with ^{64}Cu and loaded with gold nanorods for spotting small malignant masses via PET imaging and for guiding radiation therapy via CT. The presence of gold nanorods could locally enhance the efficacy of radiation therapy, limiting side effects and radiation doses. The same nanoconstructs could also slowly release locally one or more chemotherapeutic drugs to ameliorate the efficacy of the radiation therapy. In another possible configuration, ^{64}Cu-tagged discoidal nanoconstructs could be loaded with USPIOs and exposed to focused alternating magnetic fields to induce local hyperthermia and enhance blood perfusion and vessel permeability. In addition, conventional spherical NPs, loaded with chemotherapeutic molecules, could more efficiently accumulate deeper into the tumor matrix, upon systemic injection. Indeed, the possible combinations are limited only by the available resources and clinical needs.

In conclusion, it should be emphasized that nanoconstructs will always appear more complicated and more difficult to handle than single molecules in the eyes of

pharmaceutical companies, approval agencies, and some scientists. But the opportunities to be derived from merging, in a single entity, multiple imaging modalities and different therapeutic strategies are offered only by nanoparticles, and more effort should be dedicated to developing nanoconstructs for theranosis in pulmonary cancers.

Acknowledgments The authors would like to thank Dr. Henry Dirk Sostman for useful discussion. This work was partially supported by the Cancer Prevention Research Institute of Texas through the Grant CPRIT RP110262; the US National Cancer Institute (USA) (NIH) U54CA143837 and U54CA151668, and the European Research Council under the European Union's Seventh Framework Programme (FP7/2007-2013)/ERC Grant agreement no 616695. M. Ferrari acknowledges the Ernest Cockrell Jr Distinguished Endowed Chair. The authors would like to thank M. Landry for assistance with the graphical work.

Conflict of interest The authors, Jaehong Key, Y.-S. Kim, Francesca Tatulli, Brian O'Neill, Santosh Aryal, Maricela Ramirez, Xuewu Liu, Mauro Ferrari, Reginal Munden and Paolo Decuzzi, declare no conflict of interest.

Human and Animal Studies All institutional and national guidelines for the care and use of laboratory animals were followed.

References

1. Cancer facts and figures (2014) American Cancer Society. http://www.cancer.org/research/cancerfactsstatistics/
2. Cancer (2013) Fact sheet No 297. World Health Organization. http://www.who.int/mediacentre/factsheets/fs297/en/
3. Rami-Porta R, Ball D, Crowley J, Giroux DJ, Jett J, Travis WD, Tsuboi M, Vallières E, Goldstraw P, International Staging Committee, Cancer Research and Biostatistics, Observers to the Committee, Participating Institutions (2007) The IASLC lung cancer staging project: proposals for the revision of the T descriptors in the forthcoming (seventh) edition of the TNM classification for lung cancer. J Thorac Oncol 2:593–602
4. Murphy SL, Xu J, Kochanek KD (2013) National vital statistics report. Deaths: final data for 2010. Centers for Disease Control and Prevention 61(04). http://www.cdc.gov/nchs/products/nvsr.htm
5. Howlader N, Noone AM, Krapcho M, Garshell J, Neyman N, Altekruse SF, Kosary CL, Yu M, Ruhl J, Tatalovich Z, Cho H, Mariotto A, Lewis DR, Chen HS, Feuer EJ, Cronin KA (eds) (2013) SEER cancer statistics review, 1975–2010. National Cancer Institute, Bethesda, MD. http://seer.cancer.gov/csr/1975_2010/, based on November 2012 SEER data submission, posted to the SEER web site, April 2013
6. Mohammed TL, Chowdhry A, Reddy GP, Amorosa JK, Brown K, Dyer DS, Ginsburg ME, Heitkamp DE, Jeudy J, Kirsch J, MacMahon H, Parker JA, Ravenel JG, Saleh AG, Shah RD, Expert panel on thoracic imaging (2011) ACR appropriateness criteria® screening for pulmonary metastases. J Thorac Imaging 26:W1–W3
7. Ettinger DS, Bepler G, Bueno R, Chang A, Chang JY, Chirieac LR, D'Amico TA, Demmy TL, Feigenberg SJ, Grannis FW Jr, Jahan T, Jahanzeb M, Kessinger A, Komaki R, Kris MG, Langer CJ, Le QT, Martins R, Otterson GA, Robert F, Sugarbaker DJ, Wood DE, National Comprehensive Cancer Network (NCCN) (2006) Non-small cell lung cancer clinical practice guidelines in oncology. J Natl Compr Canc Netw 4(6):548–582
8. National Lung Screening Trial Research Team, Aberle DR, Adams AM, Berg CD, Black WC, Clapp JD, Fagerstrom RM, Gareen IF, Gatsonis C, Marcus PM, Sicks JD (2011) Reduced lung-cancer mortality with low-dose computed tomographic screening. N Engl J Med 365:395–409
9. Lynch TJ, Bogart JA, Curran WJ Jr, DeCamp MM, Gandara DR, Goss G, Henschke CI, Jett JR, Johnson BE, Kelly KL, Le Chevalier T, Mulshine JL, Scagliotti GV, Schiller JH, Shaw A, Thatcher N, Vokes EE, Wood DE, Hart C (2005) Early stage lung cancer—new approaches to evaluation and treatment: conference summary statement. Clin Cancer Res 11(13 Pt 2):4981s–4983s
10. Lardinois D, Weder W, Hany TF, Kamel EM, Korom S, Seifert B, von Schulthess GK, Steinert HC (2003) Staging of non-small-cell lung cancer with integrated positron-emission tomography and computed tomography. N Engl J Med 348:2500–2507
11. Vansteenkiste JF, Stroobants SG (2004) Positron emission tomography in the management of non-small cell lung cancer. Hematol Oncol Clin North Am 18:269–288
12. Antoch G, Stattaus J, Nemat AT, Marnitz S, Beyer T, Kuehl H, Bockisch A, Debatin JF, Freudenberg LS (2003) Non-small cell lung cancer: dual-modality PET/CT in preoperative staging. Radiology 229:526–533
13. Ferrari M (2005) Cancer nanotechnology: opportunities and challenges. Nat Rev Cancer 5:161–171
14. Peer D, Karp JM, Hong S, Farokhzad OC, Margalit R, Langer R (2007) Nanocarriers as an emerging platform for cancer therapy. Nat Nanotechnol 2:751–760
15. Jain RK, Stylianopoulos T (2010) Delivering nanomedicine to solid tumors. Nat Rev Clin Oncol 7:653–664
16. Maeda H, Wu J, Sawa T, Matsumura Y, Hori K (2000) Tumor vascular permeability and the EPR effect in macromolecular therapeutics: a review. J Control Release 65:271–284
17. Decuzzi P, Pasqualini R, Arap W, Ferrari M (2009) Intravascular delivery of particulate systems: does geometry really matter? Pharm Res 26:235–243
18. Decuzzi P, Ferrari M (2008) Design maps for nanoparticles targeting the diseased microvasculature. Biomaterials 29:377–384
19. Decuzzi P, Ferrari M (2006) The adhesive strength of non-spherical particles mediated by specific interactions. Biomaterials 27:5307–5314
20. Lee TR, Choi M, Kopacz AM, Yun SH, Liu WK, Decuzzi P (2013) On the near-wall accumulation of injectable particles in the microcirculation: smaller is not better. Sci Rep 3:2079
21. Aryal S, Hu CM, Zhang L (2010) Combinatorial drug conjugation enables nanoparticle dual-drug delivery. Small 6:1442–1448
22. Key J, Aryal S, Gentile F, Ananta JS, Zhong M, Landis MD, Decuzzi P (2013) Engineering discoidal polymeric nanoconstructs with enhanced magneto-optical properties for tumor imaging. Biomaterials 34:5402–5410
23. Shen J, Xu R, Mai J, Kim HC, Guo X, Qin G, Yang Y, Wolfram J, Mu C, Xia X, Gu J, Liu X, Mao ZW, Ferrari M, Shen H (2013) High capacity nanoporous silicon carrier for systemic delivery of gene silencing therapeutics. ACS Nano 7:9867–9880
24. Ananta JS, Godin B, Sethi R, Moriggi L, Liu X, Serda RE, Krishnamurthy R, Muthupillai R, Bolskar RD, Helm L, Ferrari M, Wilson LJ, Decuzzi P (2010) Geometrical confinement of gadolinium-based contrast agents in nanoporous particles enhances T1 contrast. Nat Nanotechnol 5:815–821
25. Sethi R, Ananta JS, Karmonik C, Zhong M, Fung SH, Liu X, Li K, Ferrari M, Wilson LJ, Decuzzi P (2012) Enhanced MRI relaxivity of Gd(3 +) -based contrast agents geometrically confined within porous nanoconstructs. Contrast Media Mol Imaging 7:501–508
26. Aryal S, Key J, Stigliano C, Ananta JS, Zhong M, Decuzzi P (2013) Engineered magnetic hybrid nanoparticles with enhanced relaxivity for tumor imaging. Biomaterials 34:7725–7732

27. Gizzatov A, Key J, Aryal S, Ananta J, Cervadoro A, Palange AL, Fasano M, Stigliano C, Zhong M, Di Mascolo D, Guven A, Chiavazzo E, Asinari P, Liu X, Ferrari M, Wilson LJ, Decuzzi P (2014) Hierarchically structured magnetic nanoconstructs with enhanced relaxivity and cooperative tumor accumulation. Adv Funct Mater. doi:10.1002/adfm.201400653
28. Aryal S, Key J, Stigliano C, Landis MD, Lee DY, Decuzzi P (2014) Positron emitting magnetic nanoconstructs for PET/MR imaging. Small 10:2688–2696
29. Di Mascolo D, Lyon JC, Aryal S, Ramirez MR, Wang J, Candeloro P, Guindani M, Hsueh WA, Decuzzi P (2013) Rosiglitazone-loaded nanospheres for modulating macrophage-specific inflammation in obesity. J Control Release 170:460–468
30. Jones-Wilson TM, Deal KA, Anderson CJ, McCarthy DW, Kovacs Z, Motekaitis RJ, Sherry AD, Martell AE, Welch MJ (1998) The in vivo behavior of copper-64-labeled azamacrocyclic complexes. Nucl Med Biol 25:523–530
31. Godin B, Chiappini C, Srinivasan S, Alexander JF, Yokoi K, Ferrari M, Decuzzi P, Liu X (2012) Discoidal porous silicon particles: fabrication and biodistribution in breast cancer bearing mice. Adv Funct Mater 22:4225–4235
32. Blanco E, Sangai T, Hsiao A, Ferrati S, Bai L, Liu X, Meric-Bernstam F, Ferrari M (2013) Multistage delivery of chemotherapeutic nanoparticles for breast cancer treatment. Cancer Lett 334:245–252
33. Shen H, Mittal V, Ferrari M, Chang J (2013) Delivery of gene silencing agents for breast cancer therapy. Breast Cancer Res 15:205
34. Shen H, Rodriguez-Aguayo C, Xu R, Gonzalez-Villasana V, Mai J, Huang Y, Zhang G, Guo X, Bai L, Qin G, Deng X, Li Q, Erm DR, Aslan B, Liu X, Sakamoto J, Chavez-Reyes A, Han HD, Sood AK, Ferrari M, Lopez-Berestein G (2013) Enhancing chemotherapy response with sustained EphA2 silencing using multistage vector delivery. Clin Cancer Res 19:1806–1815
35. Gizzatov A, Stigliano C, Ananta JS, Sethi R, Xu R, Guven A, Ramirez M, Shen H, Sood A, Ferrari M, Wilson LJ, Liu X, Decuzzi P (2014) Geometrical confinement of Gd(DOTA) molecules within mesoporous silicon nanoconstructs for MR imaging of cancer. Cancer Lett. doi:10.1016/j.canlet.2014.06.001